

## applied optics

# Imaging through a homogeneous circular cylinder: the role of virtual caustics, rainbow glare points, and image fragmentation

**JAMES A. LOCK** 

Physics Department, Cleveland State University, Cleveland, Ohio 44115, USA (j.lock@csuohio.edu)

Received 13 February 2020; revised 3 May 2020; accepted 6 May 2020; posted 6 May 2020 (Doc. ID 390330); published 10 June 2020

Small air bubbles on the rear inside surface of a water-filled cylinder, near its edges, appear horizontally elongated, joined in pairs, and take on color. Similarly, if an extended object is sufficiently close to the water-filled cylinder, three images of the object are seen when looking through the cylinder. The center image joins onto the left or right image as the observer moves his or her head back and forth in front of the cylinder. The first observation is explained in terms of glare points of light, and the real and virtual parts of the external caustic of the light transmitted through the water-filled cylinder. The second observation is explained as an example of Berry's caustic touching theorem which describes the topological method of fragmentation of an object's image into multiple images. For the situation studied here, an imaginary cylindrical aberration caustic of the water-filled cylinder decomposes object space into a three-ray region sandwiched between two one-ray regions. As an extended object crosses the caustic boundary from one of the one-ray regions into the three-ray region, an image-pair creation event occurs, which is followed by an image-pair disconnection event producing the three images. Similarly, when the extended object crosses the caustic boundary from the three-ray region into one of the one-ray regions, an image-pair merging event occurs, which is followed by an image-pair annihilation event producing the one remaining image. © 2020 Optical Society of America

https://doi.org/10.1364/AO.390330

#### 1. INTRODUCTION

The goal of technological imaging, from visible light optical instruments such as microscopes and cameras to generalized imaging modalities such as radio telescopes and medical scanners, is to produce a faithful aberration-free representation of the object or visual scene being imaged. However, the images resulting from reflection by or transmission through curved or rippled surfaces in the natural environment are almost always dominated by highly distorted images and/or multiple images of the original visual scene. For example, consider the following two observations through a homogeneous circular cylinder. First, small air bubbles form on the inside surface of a waterfilled cylinder, such as a glass vase. Although air bubbles near the cylinder centerline are seen by a distant observer as having a normal size and shape, bubbles on the back surface near the edges appear horizontally elongated, joined in pairs, and take on color (see Figs. 1 and 2). Second, consider an extended object located behind the water-filled cylinder. If the object is sufficiently close to the cylinder surface, three distorted images of the object are seen when looking at it through the cylinder. Two of the images have a normal orientation, while the middle image is reversed (see Fig. 3). The reversed center image joins onto the left or right image of normal orientation as the observer moves his or her head back and forth in front of the cylinder (see Fig. 4). The same phenomenon has been observed by the author for an extended object behind a clear, smooth icicle.

The explanation of these two easily observed phenomena relies on the interplay of a number of different optical structures. The small bubbles resemble point sources, whose images as seen by an observer appear as glare points [1–5]. The location of the effective source of the glare point images lies on the real or virtual portion of the external transmission caustic of the cylinder [6–12]. The topological structure of an extended object immediately behind the water-filled cylinder, i.e., the number of complete and partial images of the object seen by the observer, is determined by Berry's caustic touching theorem [13,14]. The theorem describes an imaginary caustic produced by propagating light backward through the optical system, which is overlaid on the extended object plane. It subdivides the extended object plane into a number of different regions, corresponding to a different number of images of each of the points that comprise the extended object [15].

The body of this paper proceeds as follows. The caustic of the rays exiting a homogeneous circular cylinder following p-1 internal reflections for normal plane wave incidence is briefly



**Fig. 1.** 8.9 cm outer diameter thin-wall water-filled glass vase, with small air bubbles adhering to the inside front and rear surfaces.

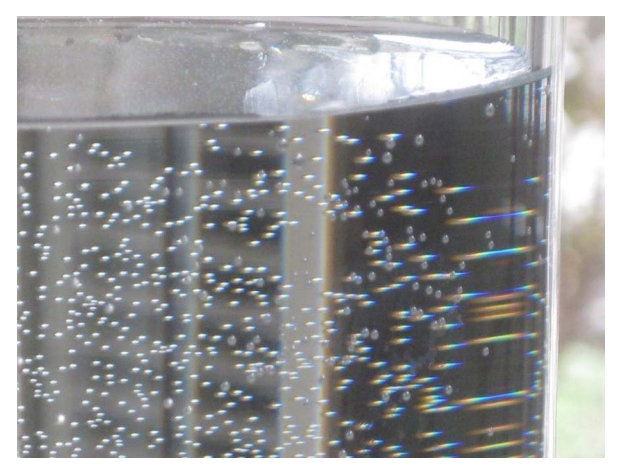


**Fig. 2.** Detailed view of the right side of Fig. 1. The two images of each air bubble on the rear inside surface close to each of the edges are elongated, joined together, take on color, and then vanish as the observer moves his or her head.

reviewed in Section 2. The real and virtual portions of the caustic are identified and discussed. The caustic of the exiting rays for an isotropic point source a finite distance from the cylinder surface is discussed in Section 3. The connection between the glare points seen by a far-zone observer and the exterior caustic of Sections 2 and 3 is described in Section 4. In Section 5, the results of Section 4 provide a simple example of the use of the caustic touching theorem to illustrate the topology of the multiple images of an extended object as seen through the cylinder. A simple topological construction which motivates the theorem and has previously been used to describe the ray structure of optical caustics [14,16], mirages [17,18], and ice crystal halos [19], is also described.

## 2. SHAPE OF THE EXTERIOR CAUSTIC FOR PLANE WAVE INCIDENCE

Consider a plane wave in an exterior medium of unit refractive index normally incident on a homogeneous circular cylinder of radius a and refractive index m as in Fig. 5. The symmetry axis



**Fig. 3.** Three images of an electric candle placed 3.0 cm behind an 8.9 cm outer diameter thin-wall water-filled glass vase. The camera lens was 35 cm in front of the vase. The left and right images have normal orientation and the central image is of reversed orientation.



**Fig. 4.** The observer moves his or her head to the left or right, two of the three images seen in Fig. 3 merge together.

of the cylinder coincides with the z axis of a rectangular coordinate system. The family of parallel incident rays associated with a plane wave propagates in the positive x direction in the xy plane. An incident ray makes an angle of incidence  $\theta_i$  at the cylinder surface, with  $-90^{\circ} \le \theta_i \le 90^{\circ}$ . The ray refracts into the cylinder, makes p-1 internal reflections inside with  $p \ge 1$ , and then refracts back out at the deflection angle  $\Theta$  with respect to the incident direction of travel, measured clockwise with respect to the positive x axis as in Fig. 5. The deflection angle is

$$\Theta = (p-1)\pi + 2\theta_i - 2p\theta_t,$$
 (1)

where the angle of refraction at the cylinder surface,  $\theta_t$ , is given by Snell's law,

$$\sin(\theta_i) = m\sin(\theta_t). \tag{2}$$

For  $p \ge 1$ , the scattering angle of the axial ray (A) with  $\theta_i^A = 0^\circ$  is

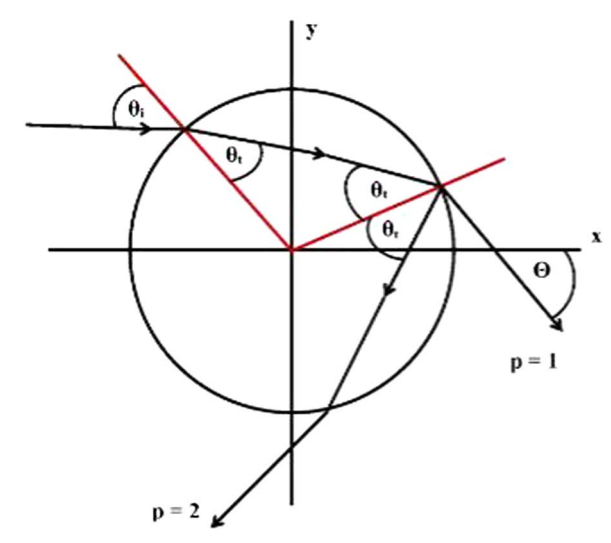


**Fig. 5.** Rays transmitted through the cylinder (p = 1), and exiting the cylinder after one internal reflection (p = 2).

$$\Theta^A = (p-1)\pi, \tag{3}$$

and the critical scattering angle of the grazing incident ray (C) with  $\theta_i^{\ C}=90^\circ$  is

$$\Theta^C = p\pi - 2p\theta_t^C, \tag{4}$$

where

$$\theta_t^C = \arcsin(1/m). {(5)}$$

For  $p \ge 2$  a rainbow (R) occurs at the relative minimum of  $\Theta(\theta_i)$  when

$$\sin(\theta_i^R) = [(p^2 - m^2)/(p^2 - 1)]^{1/2}.$$
 (6)

For p=1, the deflection angle monotonically increases from  $\Theta^A=0^\circ$  to  $\Theta^C$  as  $\theta_i$  increases from  $0^\circ$  to  $90^\circ$ . For p=2, the deflection angle decreases from  $\Theta^A=180^\circ$  to  $\Theta^R$ , and then increases back to  $\Theta^C$  as  $\theta_i$  increases from  $0^\circ$  to  $90^\circ$ . For m=4/3 and p=1,  $\Theta^C=82.82^\circ$ . For p=2,  $\Theta^R=137.98^\circ$  and  $\Theta^C=165.64^\circ$ . When  $m>2^{1/2}$ ,  $\Theta^C$  for p=2 is greater than  $180^\circ$ .

When the exiting rays corresponding to neighboring values of  $\theta_i$  converge toward each other in the scattering near-zone and then cross, the envelope of all the crossings is the real portion of the exterior caustic for p-1 internal reflections. This portion of the caustic is called exterior because it is formed by the rays that have exited the cylinder and are in the surrounding external medium. It is called real since it is a narrow region of greatly amplified light intensity due to partial focusing which can be seen by an observer on a viewing screen that intersects the caustic. On the other hand, sometimes the exiting rays corresponding to neighboring values of  $\theta_i$  diverge from each other throughout the scattering near-zone. The backward extrapolation of the ray paths cross each other either inside the cylinder or in the exterior medium on the other side of it. This is not to be confused with the interior caustic produced by the crossing of the rays refracted inside the cylinder [20]. The envelope of the crossings of the backward extrapolation of the exterior rays is called the virtual portion of the exterior caustic for p-1 internal reflections. (For p=2 see, for example, Fig. 174 of [6] which is also reproduced as the cover illustration, Fig. 61 of [7], and Fig. 7 of [8]). As is the case for a virtual image of an object produced by a mirror or a thin lens (see Sec. 34.2 of [21] and p. 481 of [22]), the virtual portion of the caustic is not a narrow region of intensity amplification and does not illuminate a viewing screen placed at its location. Rather, a different observable physical manifestation the virtual caustic will be described in Section 4.

The shape of the real plus virtual portions of the exterior p-1 internal reflection caustic for plane wave incidence are well known (for the p=1 caustic, see either Fig. 6 here or [9], and for the p=2 caustic, see either Fig. 7 here or [6–8,10,11]). These caustics are briefly reviewed here in order to set the stage for the analysis of Sections 3 and 4. The shape of the p-1 internal reflection exterior caustic as a function of  $\theta_i$  for  $0^\circ \le \theta_i \le 90^\circ$  is given by [9,12]

$$x/a = \sin(\theta_i)\sin(\Theta) + L(\theta_i)\cos(\theta_i)\cos(\Theta),$$
 (7a)

$$y/a = \sin(\theta_i)\cos(\Theta) - L(\theta_i)\cos(\theta_i)\sin(\Theta),$$
 (7b)

where

$$L(\theta_i) = (d\Theta/d\theta_i)^{-1} = (1/2) \left\{ 1 - [p\cos(\theta_i)]/[m\cos(\theta_i)] \right\}^{-1}.$$
(8)

All points on the caustic can be parameterized either by their value of  $\theta_i$  or by their value of  $\Theta$ . The polar coordinates  $(r, \varphi)$  of a point on the caustic are

$$r/a = (x^2 + y^2)^{1/2}/a = 1 + [L(\theta_i)^2 - 1]\cos(\theta_i),$$
 (9a)

$$\tan(\varphi) = [\tan(\theta_i) - L(\theta_i) \tan(\Theta)] / [L(\theta_i) + \tan(\theta_i) \tan(\Theta)],$$
**(9b)**

where the angle  $\varphi$  is measured counterclockwise with respect to the positive x axis of Fig. 5. From Eq. (5a), the caustic crosses the cylinder surface (S) either when  $L(\theta_i^{S\pm}) = \pm 1$  or when  $\theta_i^C = 90^\circ$ . For example,  $L(\theta_i^{S-}) = -1$  occurs for  $p \ge 2$  when

$$\sin(\theta_i^{S-}) = [(4p^2 - 9m^2)/(4p^2 - 9)]^{1/2},$$
 (10a)

leading to

$$\varphi = -(\theta_i^{S-} + \Theta^{S-}). \tag{10b}$$

The caustic also crosses the cylinder surface at  $L(\theta_i^{S+}) = +1$  for  $p \ge 1$  when

$$\sin(\theta_i^{S+}) = [(4p^2 - m^2)/(4p^2 - 1)]^{1/2},$$
 (11a)

leading to

$$\varphi = (\theta_i^{S+} - \Theta^{S+}). \tag{11b}$$

Finally, for  $p \ge 2$  the far-zone rainbow occurs for  $L(\theta_i^R) \to \pm \infty$ . If  $|L(\theta_i)| < 1$  a point on the caustic is inside the cylinder and is thus virtual. If  $|L(\theta_i)| > 1$  a point on the caustic is outside the cylinder and may be either real or virtual.

A subtle feature of the caustic is a pair of symmetrically located virtual cusps (VCs) that occur just inside the cylinder

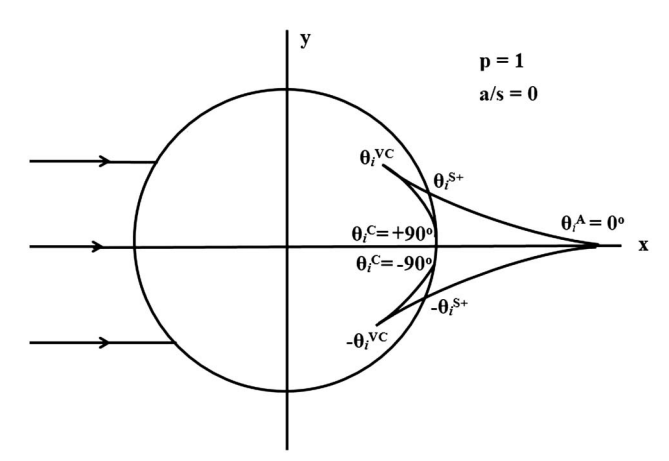


**Fig. 6.** Caustic of the transmitted rays for plane wave incidence. The size of two virtual cusps inside the cylinder has been exaggerated.

surface either above the x axis or below it, as qualitatively shown in Figs. 6 and 7 and described in [10,11]. The location of the apex point of each of the cusps can be obtained analytically by solving the cubic equation for the relative minimum of  $(r/a)^2$  inside the cylinder. For positive  $\theta_i$  the apex point is given by

$$\sin(\theta_i^{VC}) = [(p^2 - w^2 m^2)/(p^2 - w^2)]^{1/2},$$
 (12)

where for p = 1,

$$w = (3 - 5^{1/2})/2,$$
 (13a)

and for  $p \ge 2$ ,

$$u = 16p^4 - 24p^2 - 3,$$
 (13b)

$$v = 16p$$
, (13c)

$$t = (u^2 - v^2)^{1/2},$$
 (13d)

$$w = 4p^2/(4p^2 - 1) - [p^2(u - t)/2]^{1/3}/(4p^2 - 1)$$
$$- [p^2(u + t)/2]^{1/3}/(4p^2 - 1).$$
 (13e)

One of the arms of these virtual cusps begins at the cylinder surface when  $L(\theta_i^{S+})=1$ , and the other arm ends by tangentially touching another point on the cylinder surface when  $\theta_i^C=\pm 90^\circ$ . In order to illustrate how close this pair of cusp caustics is to the cylinder surface, for m=4/3 and p=1, one of the symmetrically located virtual caustics begins at r/a=1 and  $\varphi=21.03^\circ$ , the apex point is at r/a=0.9768 and  $\varphi=23.78^\circ$ , and it ends at r/a=1 and  $\varphi=7.18^\circ$ . For p=2, one of the virtual caustics begins at r/a=1 and  $\varphi=-69.19^\circ$ , the apex point is at r/a=0.9948 and  $\varphi=-67.72^\circ$ , and it ends at r/a=1 and  $\varphi=-75.64^\circ$ . Figures 6–8 are purposely not drawn to scale in order to illustrate these virtual cusps more clearly.

As is qualitatively shown in Fig. 6 for p=1, the exterior transmission caustic starts outside the cylinder on the positive x axis for  $\theta_i^A=0^\circ$ , at the apex of a real outward-pointing cylindrical aberration cusp caustic. As  $\theta_i$  increases from  $0^\circ$  to  $90^\circ$ , the cusp flares away from the x axis and crosses the cylinder surface

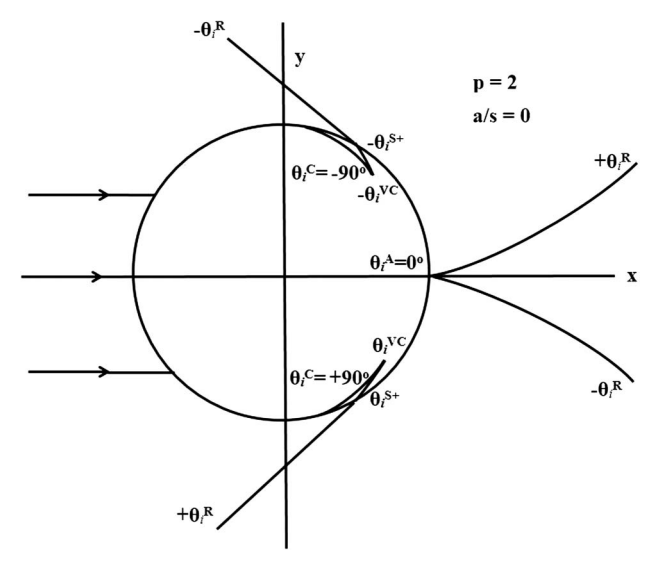


**Fig. 7.** Caustic of the one-internal-reflection rays for plane wave incidence. The size of the two virtual cusps inside the cylinder has been exaggerated.

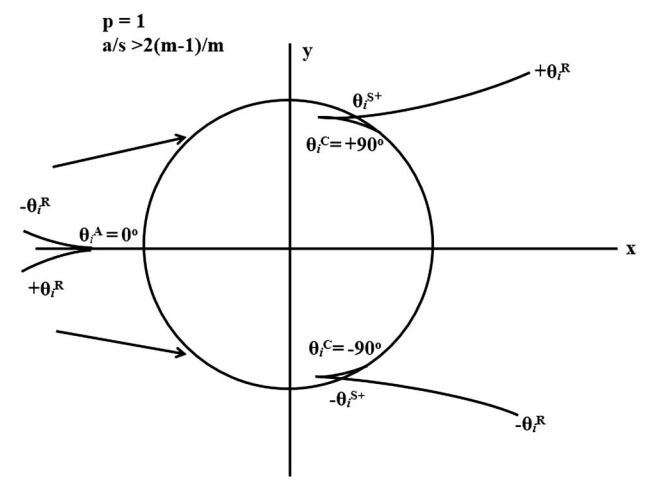


**Fig. 8.** Caustic of the transmitted rays for a near-zone isotropic point source. The size of the two virtual cusps inside the cylinder has been exaggerated.

from the outside to the inside. The caustic then becomes virtual, continuing to flare away from the x axis inside the cylinder until it reaches the apex of the interior cusp at  $\theta_i^{VC}$  of Eqs. (12) and (13). The caustic then reverses its direction along the second arm of the interior cusp and tangentially touches the cylinder surface when  $\theta_i^C = 90^\circ$ . This tangential touching provides a smooth continuation onto a caustic coinciding with the cylinder surface associated with electromagnetic surface waves [23]. The shape of the exterior caustic for negative  $\theta_i$  is a mirror image about the x axis of the positive  $\theta_i$  caustic. Thus the complete p=1 exterior caustic has only one branch, consisting of a virtual cusp portion just inside the cylinder surface below the x axis for  $-90^\circ \le \theta_i \le -\theta_i^{S+}$ , connected to an outward-pointing real cusp portion about the positive x axis exterior to the cylinder for  $-\theta_i^{S+} \le \theta_i \le \theta_i^{S+}$ , which is in turn connected to the second

virtual cusp portion just inside the cylinder surface above the *x* axis for  $\theta_i^{S+} \le \theta_i \le 90^\circ$ .

As is qualitatively shown in Fig. 7 for p = 2, the exterior one-internal-reflection caustic starts at the cylinder surface on the positive x axis for  $\theta_i^A = 0$  at the apex of a virtual inwardpointing cusp caustic. As  $\theta_i$  increases from  $0^{\circ}$  to  $\theta_i^R$ , the cusp flares away from the x axis and extends out to infinity. Also, at  $\theta_i^R$ , a real portion of the caustic starts at infinity in the opposite direction at the far-zone Descartes first-order rainbow angle. As  $\theta_i$  continues to increase toward 90°, the rainbow caustic comes in from infinity toward the scattering near-zone, gently curving away from its asymptote and crossing the cylinder surface from the outside to the inside at  $\theta_i^{S+}$ . It then becomes virtual and continues to gently curve until it reaches the apex of the interior cusp at  $\theta_i^{\text{VC}}$ . The caustic then reverses its direction along the second arm of the interior cusp and tangentially touches the cylinder surface when  $\theta_i = 90^\circ$ . The shape of the caustic for negative  $\theta_i$  is again a mirror image about the x axis of the positive  $\theta_i$  caustic. Thus the complete p=2 exterior caustic has three distinct branches: (i) an interior virtual cusp branch just inside the cylinder surface above the x axis for  $-90^{\circ} \le \theta_i \le -\theta_i^{S+}$  that is connected to the real rainbow caustic above the *x* axis for  $-\theta_i^{S+} \le \theta_i \le -\theta_i^{R}$ ; (ii) an inward-pointing virtual cusp branch about the positive x axis outside the cylinder for  $-\theta_i^R \le \theta_i \le \theta_i^R$ ; and finally (iii) a real rainbow caustic branch below the x axis for  $\theta_i^R \le \theta_i \le \theta_i^{S+}$  that is connected to a virtual cusp caustic just inside the cylinder below the x axis for  $\theta_i^{S+} \leq \theta_i \leq 90^\circ$ .

## 3. SHAPE OF THE EXTERIOR CAUSTIC DUE TO A NEAR-ZONE SOURCE

Consider now an isotropic line source on the negative x axis of Fig. 5, parallel to the cylinder's symmetry axis a distance s > a from the center of the cylinder. The scattered angle of the rays that have undergone p-1 internal reflections before exiting the cylinder is [9,12]

$$\Theta = (p-1)\pi + 2\theta_i - 2p\theta_t - \arcsin[(a/s)\sin(\theta_i)]$$
 (14)

for  $-90^{\circ} \le \theta_i \le 90^{\circ}$  and  $0 \le a/s \le 1$ . The incident plane wave of Section 2 is the a/s = 0 limit of Eq. (14), and a line source lying on the cylinder surface is the a/s = 1 limit. Scattering by an interior source with a/s > 1 was studied in [24,25] and will not be considered here. For  $0 \le a/s \le 1$ , the coordinates of the caustic of the exterior rays for p-1 internal reflections is given by Eqs. (7a) and (7b) with

$$L(\theta_i) = (d\Theta/d\theta_i)^{-1}$$

$$= (1/2) \left\{ 1 - [p\cos(\theta_i)]/[m\cos(\theta_t)] - (1/2) (a/s)\cos(\theta_i) \left[ 1 - (a/s)^2 \sin^2(\theta_i) \right]^{-1/2} \right\}^{-1}.$$
(15)

For p = 1 and a/s < 2(m-1)/m, the external transmission caustic has an outward-pointing cusp centered about the positive x axis, as was the case in Fig. 6. When a/s = 2(m-1)/m the cusp point moves out to infinity, and for a/s > 2(m-1)/m it opens up into a real transmission rainbow caustic [9].

Simple expressions for various transition points of the caustic exist for an arbitrary value of p when a/s = 1/m or a/s = 1. For a/s = 1/m, the caustic crosses the cylinder surface for the first time at  $L(\theta_i^{S-}) = -1$  when

$$\sin(\theta_i^{S-}) = \{[(2p+1)^2 - m^2]/[(2p+1)^2 - 1]\}^{1/2},$$
 (16)

a far-zone rainbow occurs for  $|L(\theta_i^R)| \to \infty$  when

$$\sin(\theta_i^R) = \{[(2p+1)^2 - 4m^2]/[(2p+1)^2 - 4]\}^{1/2},$$
 (17)

and the caustic crosses the cylinder surface a second time at  $L(\theta_i^{S+}) = +1$  when

$$\sin(\theta_i^{S+}) = \{[(2p+1)^2 - 9m^2]/[(2p+1)^2 - 9]\}^{1/2}.$$
 (18)

For a/s = 1 the caustic crosses the cylinder surface for the first time at  $L(\theta_i^{S-}) = -1$  when

$$\sin(\theta_i^{S-}) = [(p^2 - m^2)/(p^2 - 1)]^{1/2},$$
 (19)

a far-zone rainbow occurs for  $|L(\theta_i^R)| \to \infty$  when

$$\sin(\theta_i^R) = [(4p^2 - m^2)/(4p^2 - 1)]^{1/2},$$
 (20)

and the caustic crosses the cylinder surface a second time at  $L(\theta_i^{S+}) = +1$  when  $\theta_i^{S+} = \theta_i^{C} = 90^{\circ}$ .

The p=1 transmission caustic for a/s > 2(m-1)/m is qualitatively shown in Fig. 8. It starts at  $\Theta^A = 0^\circ$  at the apex of an inward-pointing virtual cusp about the negative x axis. As  $\theta_i$  increase from  $0^\circ$  to  $\theta_i^R$ , the caustic gently curves away from the x axis and moves out to infinity in the negative x direction at  $\theta_i^R$ . Also, at  $\theta_i^R$  a real rainbow caustic comes in from infinity in the opposite direction toward the near-zone and intersects the cylinder surface at  $\theta_i^{S+}$ . At this point the caustic changes from real to virtual, and continues to gently curve just inside the cylinder surface, turning around at the interior cusp apex at  $\theta_i^{VC}$ , and proceeds back along the second arm of the interior cusp, tangentially touching the cylinder surface again when  $\theta_i^C = 90^\circ$ .

As  $a/s \rightarrow 1$ , the virtual cusp caustics just inside the cylinder surface shrink in size. For a surface source with a/s = 1, the size of each of the virtual cusps shrinks to a single point located at  $\theta_i^C = 90^\circ$ . The p = 1 exterior transmission caustic for a/s = 1 has three distinct branches: (i) a real rainbow caustic branch below the x axis for  $-90^\circ \le \theta_i \le -\theta_i^R$ , (ii) an inward-pointing virtual cusp branch about the negative x axis for  $-\theta_i^R \le \theta_i \le \theta_i^R$ , and (iii) a real rainbow caustic branch above the x axis for  $\theta_i^R \le \theta_i \le 90^\circ$ .

### 4. GLARE POINTS

Instead of having the scattered fields illuminate a far-zone viewing screen at the scattering angle  $\Theta$ , let a far-zone observer at  $\Theta$  focus his eyes in the vicinity of the scattering cylinder. The rays from a point source entering the observer's eyes make a small angle with respect to each other, and the observer perceives the source of those rays to be the position where they converge, be it a real source or a virtual one (see [21] and p. 481 of [22]). The observer at  $\Theta$  will see a number of bright glare points from rays that have undergone p-1 internal reflections before exiting the cylinder [2,3] (see also Plate III.1 of [1]). The effective source of

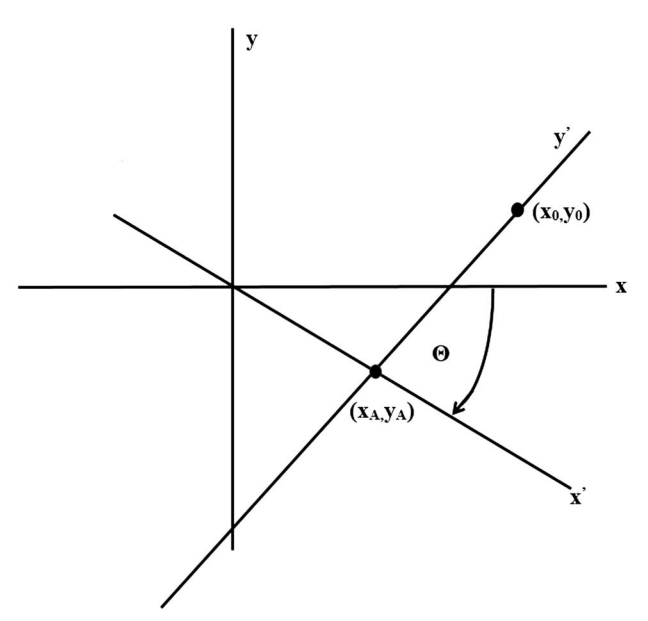


**Fig. 9.** Orientation of the x'y' coordinate system with respect to the xy coordinate system of Fig. 5.

the bright glare points is either on the real portion or the virtual portion of the exterior caustic for p-1 internal reflections, since the exterior caustic is the locus of points at which adjacent scattered rays, or their back projections, cross each other.

When an observer's eye focuses on a distant visual scene, the retina coincides with the focal plane of the eye lens. The fields emanating from the distant visual scene and incident on the eye lens are Fourier transformed at the retina (see Sec. 5.2 of [15]). When the observer focuses his or her eyes on the distant cylinder, the intensity as a function of the position on the retina is obtained by (i) computing the Fourier transform of the scattered electric field incident on the lens of the observer's eye in a small interval centered on  $\Theta$  and windowed by the size of the pupil of the observer's eye, and then (ii) taking the magnitude-squared of the result [4,5].

To find the locations of a glare point on the retina of a far-zone observer at the scattering angle  $\Theta$ , consider a new x'y' coordinate system of Fig. 9. The x' axis joins the origin of coordinates and the observer, and the y' axis is perpendicular to the x' axis and contains the arbitrary point ( $x = x_0, y = y_0$ ) in the original coordinate system. The choice of  $x_0$  and  $y_0$  will be described below. The origin of the new coordinate system is at the point ( $x = x_4, y = y_4$ ) in the original coordinate system. Thus,

$$x_A = \cos^2(\Theta) x_0 - \sin(\Theta) \cos(\Theta) y_0,$$
 (21a)

$$y_A = -\sin(\Theta)\cos(\Theta) x_0 + \sin^2(\Theta) y_0.$$
 (21b)

The image of the y' axis appears on the observer's retina. The distance along the y' axis from  $(x_A, y_A)$  to  $(x_0, y_0)$  is

$$d = x_0 \sin(\Theta) + y_0 \cos(\Theta). \tag{22}$$

Now let  $(x_0, y_0)$  be the point on the exterior caustic corresponding to the observer's angular position  $\Theta$ , and the incident

angle  $\theta_i$  associated with it. The lateral position on the observer's retina of the effective real or virtual source of the glare point is then

$$d/a = \sin(\theta_i), \tag{23}$$

independent of the shape of the caustic and whether it is real or virtual.

The evolution of the lateral location of the glare points as a function of the deflection angle  $\Theta$  can be easily demonstrated by three simple examples. First, for plane wave incidence, a/s = 0, the p = 1 glare point begins on the symmetry axis of the cylinder when the observer is at  $\Theta^A = 0^\circ$ . It monotonically migrates to the cylinder surface according to Eq. (23) as the observer moves to the critical deflection angle  $\Theta^C$  of the grazing incident ray. If the observer were to continue to move to larger  $\Theta$ , the p = 1 glare point would vanish (ignoring the persistence of an ever-weaker glare point at d/a = 1 due to electromagnetic surface waves [23]). The observed p = 1 glare point lies on the real portion of the exterior caustic of Fig. 6 for  $0^{\circ} \leq \Theta \leq \Theta^{S+}$ and on the virtual portion for  $\Theta^{S+} \leq \Theta \leq \Theta^{C}$ . The glare point evolution for negative values of  $\theta_i$  and  $\Theta$  is the same, but opposite in sign. The observation of glare point images of a localized source is the physical manifestation of the virtual portion of the exterior caustic alluded to in Section 2. If the observer's eye is dark-adapted with a larger pupil size, a more extended portion of the caustic source will be visible [26].

As a second example, for a/s = 0 and  $m < 2^{1/2}$ , the lower supernumerary p = 2 glare point begins on the cylinder axis when the observer is at  $\Theta^A = 180^\circ$ . As the observer moves to smaller  $\Theta$ , the glare point migrates away from the axis of the cylinder according to Eq. (23) until the observer is at  $\Theta^C$  when the original p = 2 glare point is joined by a new upper supernumerary p = 2 glare point at the edge of the cylinder [1–3]. This new glare point may be interpreted either as a 0-to-1 glare point transition due to the aperture effect of the edge of the cylinder (see pp. 26, 123, 133 of [14]) or a 0-to-2 glare point transition with the tunneling ray [27]. As the observer moves to yet smaller  $\Theta$ , the lower and upper supernumerary glare points approach each other, coalesce, and vanish when the observer reaches the Descartes rainbow angle  $\Theta^R$ . This evolution is shown in plate III.1 of [1]. The 2-to-0 transition will hereafter be called a glare point-pair annihilation event (gppa). If the observer were to continue to move to yet smaller  $\Theta$ , no p = 2 glare points would be seen. The lower supernumerary glare point is on the virtual part of the exterior caustic for its entire traverse. The upper supernumerary glare point is on the virtual portion of the exterior caustic from its first appearance at  $\Theta^{C}$  until  $\Theta^{S+}$ , and it is on the real portion from  $\Theta^{\bar{S}+}$  until the glare point-pair annihilation event at  $\Theta^R$ . If the observer were instead to cross the Descartes rainbow angle from smaller  $\Theta$  to larger  $\Theta$ , two coincident glare points would suddenly appear in a 0-to-2 glare point transition at  $\Theta^R$  and then recede away from each other. This will be called a glare point-pair creation event (gppc). The glare point evolution for negative values of  $\theta_i$  and  $\Theta$  is the same, but opposite in sign.

As a third example, the case of the p=1 glare points for a/s=1 directly pertains to the observation of small bubbles clinging to the back inside surface of a water-filled glass vase as in Figs. 1 and 2. Each small bubble can be considered as an

effective point source on the cylinder surface. The details of the evolution of the p = 1 glare points as a function of the observer's position  $\Theta$  are found to be exactly analogous to the case of p = 2 and a/s = 0 described in the second example above. As  $\theta_i$ increases from  $0^{\circ}$  to  $90^{\circ}$ , the p = 1 deflection angle  $\Theta$  decreases from  $\Theta^A = 0^\circ$  to the negative rainbow angle  $\Theta^R$ , and then increases back to  $\Theta^C$ , which is negative as well. For example, for m = 4/3,  $\Theta^R = -21.01^\circ$ , and  $\Theta^C = -7.18^\circ$ . As a result, when the observer is at  $\Theta = 0^{\circ}$ , the p = 1 glare point begins on the cylinder axis. We call this glare point 1. As the observer moves to negative  $\Theta$ , glare point 1 migrates away from the cylinder axis according to Eq. (23) until the observer is at  $\Theta^C$ , when it is joined by a second glare point at the edge of the cylinder, that will hereafter be called glare point 2. As the observer moves to more negative  $\Theta$ , the two glare points approach each other, coalesce, and vanish at the 2-to-0 glare point-pair annihilation event at the rainbow angle,  $\Theta^R$ . If the observer were to continue to move to yet more negative values of  $\Theta$ , no p = 1 glare points would be seen. The lower supernumerary glare point is always on the virtual portion of the exterior caustic, and the upper supernumerary glare point is always on the real portion.

In the three glare point evolutions described above, the localized source position has been fixed and the observer moves to different values of  $\Theta$ . This is called the active point of view of the evolution. One could just as well employ the passive point of view where the observer's position is fixed and the localized source is moved from place to place. Figures 1 and 2 show many small bubbles on the rear inner surface of the cylinder, corresponding to many different point source locations on the cylinder surface. Thus, in the passive point of view, they exhibit many stages of the evolution of the p = 1 glare points, from the axial images to the glare point-pair creation and annihilation events near the edge of the cylinder. This is the exact analogy of the familiar merging of the p = 2 glare point image for an incident plane wave as described in [2,3] and photographed in Plate III.1 of [1]. The glare point pairs take on color near their merging because the refractive index of water, and thus the rainbow angle of Eq. (20), depends on the wavelength of the incident light. Although only the p = 1 and p = 2 glare points are discussed here, it should be noted that glare points up to p = 14 were observed in [2,3], and using a thin stream of falling water, Félix Billet observed glare spots up to p = 20 in 1868, as described on p. 309 of [7].

## 5. IMAGING OF AN EXTENDED OBJECT BY A CYLINDER

The evolution of the p=1 glare points exhibits an additional feature if the point source is located a small distance beyond the cylinder surface. For example, consider m=4/3 and a/s=1/m=3/4. When  $\theta_i^A=0^\circ$ , the deflection angle is  $\Theta^A=0^\circ$ . As  $\theta_i$  increases from  $0^\circ$  to  $\theta_i^R$ , the deflection angle decreases until it reaches a relative minimum at the transmission rainbow  $\Theta^R=-6.49^\circ$ . As  $\theta_i$  increases further from  $\theta_i^R$  to  $90^\circ$ , the deflection angle increases to  $\Theta^C=+34.23^\circ$ . An identical evolution occurs as  $\theta_i$  varies between  $0^\circ$  and  $-90^\circ$ . The deflection angle again starts out at  $0^\circ$  and increases until it reaches a relative maximum at  $-\Theta^R=+6.49^\circ$ . It then decreases to  $-\Theta^C=-34.23^\circ$  when  $\theta_i=-90^\circ$ .

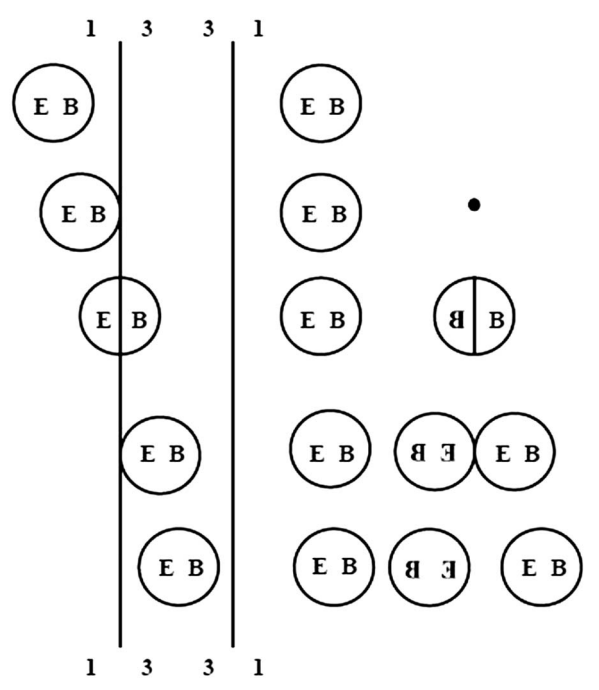


**Fig. 10.** As an extended object moves across the 1-to-3-ray imaginary caustic boundary (left), the image of the extended object (right) evolves from a single image of normal orientation, to a single image plus two partial images of normal and reversed orientation joined back-to-back, to three complete images. The left and right images have normal orientation and the central image is of reversed orientation.

This is the exact analogy of the behavior of the deflection angle for p=2 and  $m>2^{1/2}$ , for which  $\Theta^C>180^\circ$ , as was mentioned in Section 2, and which exhibits a 1-to-3-to-1 glare point transition as is illustrated in Fig. 10 of [28]. For the near-zone source being discussed here, an observer moving from negative  $\Theta$  to positive  $\Theta$  sees no p=1 glare points for  $\Theta < -\Theta^C$ . At  $\Theta = -\Theta^C$  a glare point corresponding to the grazing incidence ray appears on the observer's retina at the edge of the cylinder. It will again be referred to as glare point 1, and can be interpreted either as an aperture effect or a 0-to-2 glare point transition with the tunneling ray. For  $-\Theta^C \leq \Theta < -|\Theta^R|$ , glare point 1 starts moving away from the cylinder surface. At  $\Theta = -|\Theta^R|$ , a glare point-pair creation event occurs at which two new coincident glare points, called 2 and 3, suddenly appear at another location on the observer's retina. For  $-|\Theta^R| < \Theta < |\Theta^R|$  there are now three glare points with glare point 2 receding away from glare point 3 and approaching glare point 1. At  $\Theta = |\Theta^R|$  a glare point-pair annihilation event occurs at which glare points 1 and 2 coincide and vanish. For  $|\Theta^R| < \Theta < \Theta^C$  only glare point 3 remains. Finally, no glare points are observed for  $\Theta > \Theta^C$ .

This result helps to understand the structure of the image on the observer's retina if an extended object, rather than a single point source, were placed behind the cylinder near its surface. Since an extended object can be mathematically decomposed into a collection of neighboring point sources of differing brightness (see Sec. 2.2 of [15]), some points will have one image while other points will have three images. The way in which this occurs is described by the caustic touching theorem [13]. As in

the observations of Figs. 3 and 4, light leaving the plane containing the extended object first passes through the distorting medium (i.e., the water-filled cylinder). It is then incident on the lens of the eye of a distant observer, and is finally imaged with distortion and/or fragmentation on the observer's retina. The caustic touching theorem suggests that one consider what would happen if an imaginary point source was placed on the observer's retina, and the light from it propagated in the reverse direction through the optical system described above, ending up at the extended object plane. Light from the imaginary point source, after passing through the eye lens, would be converted into a plane wave that would then be transmitted through the water-filled cylinder in the reverse direction, and would give rise to an imaginary cylindrical aberration transmission caustic that intersects the extended object plane if it were sufficiently close to the cylinder. The intersection would take the form of two parallel boundaries between two one-ray regions and the three-ray region between them. When this imaginary caustic is overlaid on the extended object, the number of imaginary rays passing through each point of the extended object is equal to the number of images of that point on the observer's retina.

The structure of the image of the extended object can be straightforwardly determined using the following procedure. One starts with the extended object initially located in one of the one-ray regions of the extended object plane (see Fig. 10). This produces a single (possibly distorted) image of the extended object of normal orientation on the observer's retina, hereafter called image 1 (first row of Fig. 10). One then moves the extended object from its initial location to its intended location and watches how the topology of the image changes along the extended object's path. One terminates this procedure when the extended object reaches its intended location.

The topology of the image changes for the first time via an image-pair creation event (IPC) when the first point on the extended object touches the imaginary caustic boundary between the initial one-ray region and the three-ray region (second row of Fig. 10). In addition to image 1 that will remain as a spectator, two new coincident images of the touching point of the extended object, hereafter called 2' and 3, suddenly appear at a different location on the observer's retina. As more of the extended object moves across the imaginary caustic boundary into the three-ray region, the two images of the portion of the extended object now in the three-ray region are joined back-toback, appearing to grow outward from an effective source along their join-line (third row of Fig. 10). One of the partial images, 3, is of normal orientation and the other, 2', is of reversed orientation. The image topology changes for a second time via an image-pair disconnection event (IPD) when the last point on the extended object touches the imaginary caustic boundary (fourth row of Fig. 10). At this condition, images 2' and 3 on the observer's retina are now complete but are attached to each other at a single point. Once the extended object moves into the three-ray region of the imaginary caustic, the single-point connection breaks and one is left with three complete images of the extended object, 1, 2', and 3 (fifth row of Fig. 10). The image-pair creation sequence from IPC to IPD for the image of an extended object is the analog of the gppc for the image of a point source.

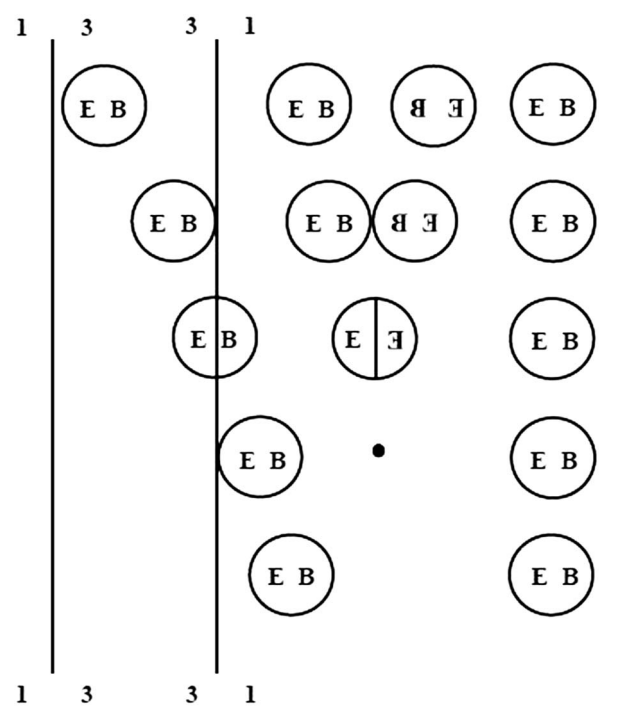


**Fig. 11.** As an extended object moves across the 3-to-1-ray imaginary caustic boundary (left), the image of the extended object (right) evolves from three complete images, to a single image of normal orientation plus two partial images of normal and reversed orientation joined back-to-back, to a single complete image of normal orientation.

At this point in the image evolution, image 2' lies between images 1 and 3 on the observer's retina. If the extended object were to continue to move toward the other imaginary caustic boundary between the three-ray region and the second one-ray region, image 2' would recede away from image 3 and approach image 1 (first row of Fig. 11). The topology of the image changes via an image-pair merging event (IPM), when the first point on the extended object touches this second imaginary caustic boundary. At this condition, the images of 1 and 2' join together at a single point on the observer's retina, with image 3 remaining as a spectator (second row of Fig. 11). As more of the extended object moves across the imaginary caustic boundary from the three-ray region into the second one-ray region, identical portions of image 1 and 2' are joined together back-to-back, appearing to vanish into an effective sink along the join-line (third row of Fig. 11). The image topology changes for the last time via an image pair annihilation event (IPA) when the last point on the extended object touches the second imaginary caustic boundary. At this condition, the two back-to-back images on the observer's retina have shrunk down to a single point (fourth row of Fig. 11). Once the extended object moves totally into the second one-ray region of the imaginary caustic, the single point image-pair vanishes and one is left with only image 3 that was previously created in the sequence between IPC and IPD (fifth row of Fig. 11). The image-pair annihilation sequence from IPM to IPA for the image of an extended object is analogous to the gppa for the image of a point source.

This is the sequence of topology-changing events by which the original image 1 is replaced by the final image 3 via the exchange of the reversed image 2'. It should be noted that event IPA becomes event IPC and event IPM becomes event IPD if the image evolution path of the extended object were to be reversed. The images take on additional color at the events IPA, IPC, IPD, and IPM because the refractive index of the cylinder, and thus the location of the imaginary cylindrical aberration caustic in the extended object plane, depends on the wavelength of the incident light.

If the distorting medium was more complicated so that its imaginary transmission caustic overlaid on the extended object plane contained a cusp point, the image evolution would be more complicated as well. Initially the extended object is in the one-ray region of the overlaid imaginary caustic, and its single image on the observer's retina is hereafter called 1. It is assumed that the path of the extended object from its initial location to its intended location proceeds through the imaginary cusp point. When the first point on the extended object touches the cusp point, three new images of the touching point on image 1, hereafter called 2, 3', and 4, are created at the location of the touching point, and replace it on the observer's retina. As progressively more of the extended object enters the three-ray region through the cusp point, the three new partial images 2, 3', and 4 grow out of the correspondingly shrinking portion of the original image 1 that is still in the one-ray region, giving a total of four partial images connected together. As the extended object crosses completely into the three-ray region of the overlaid imaginary caustic, the original image 1 shrinks to a point and vanishes. The three new images 2, 3', and 4 disconnect from each other, producing the three final images on the observer's retina. This situation is analyzed in detail in [13] and will not be discussed further here.

The propagation of light from the extended object plane through the distorting medium and the lens of the eye of the observer to the retinal plane defines a mapping T between the extended object plane coordinates  $(x_e, y_e)$  and the retinal plane coordinates  $(x_r, y_r)$ . The distortions of the image on the observer's retinal plane cannot be quantitatively determined unless one either measures or models the specific form of the mapping T. However, changes in the topology of the image, such as the number of complete or partial images of a given extended object, can occur in only a limited number of ways. Examples are (i) the 0-to-2 and 2-to-0 transitions in Figs. 1 and 2, for an inferior mirage (see Fig. 7.8 of [29]), or for reflections of objects from the curved metal surface of an automobile, and (ii) the replacement of image 1 by image 3 via the exchange of image 2' in the 1-to-3-to-1 transition described earlier in this section. The power of the caustic touching theorem [13] is that it provides a way of cataloging these universal modes of image fragmentation. For example, the 1-to-3-to-1 transition has also been observed in superior mirages (see pp. 163–165 of [29]) and glints reflected from the surface of water waves [30,31]. In addition, large image distortions are produced and then inverted in anamorphic art (see pp. 79-83 of [32]). As far as technological applications are concerned, image fragmentation is used as an observational tool in gravitational lensing (see, for example, [33,34]).

The details of the 0-to-2 transition of Figs. 1 and 2 and the 1-to-3-to-1 transition of Figs. 3 and 4 can be motivated by a geometrical construction that has been previously used to explain

mirages [17,18], ice crystal halos [19], and the ray structure of caustics ([16] and Sec. 2.6 of [14]). The mapping T from the extended object plane to the image plane is frequently highly nonlinear and may lack a unique inverse in certain regions. As an alternative, one can choose to put all the complexity into a highly distorted image plane with T now being the identity operator between the initial extended object plane and the new distorted image plane. The lack of a unique inverse of the mapping is accommodated by folding part of the image plane over on itself.

Consider, for example, the 0-to-2 transition where the action of T on  $(x_e, y_e)$  in the extended object plane results in either two points  $(x_r, y_r)$  in the image plane, or no points. A simple one-dimensional model of this transition is the parabola  $y = x^2$ where two values of the independent variable x are mapped into each value of the dependent variable y for y > 0, and no values of x are mapped into y for y < 0. Now consider the inverse of this function where one knows  $\gamma$  and wants to find x. There are either two solutions or none. The original parabola, now viewed from the side, gives the appearance of being folded over on itself. In like manner, all points that comprise an extended object will have either two images or no images, depending on which side of the fold-line where the distorted image plane is folded over on itself, the point occurs on. If the extended object is initially completely in the no-image portion of the  $(x_e, y_e)$  plane and is moved along a path to the two-image portion, first, an IPC event occurs. Then two partial images of the extended object appear back-to-back in the  $(x_r, y_r)$  plane, joined by fold-line. The partial image on the upper surface of the folded image plane is of normal orientation, and the partial image on the lower surface is of reversed orientation. As the extended object continues along its path, an IPD event occurs where the two complete images on the folded image plane separate from each other.

For a mapping T that contains a 1-to-3-to-1 transition, the action of T on  $(x_e, y_e)$  results in either one or three points  $(x_r, y_e)$  $y_r$ ). A simple one-dimensional model of this transition is the cubic function  $y = x^3 - x$  where three values of the independent variable x are mapped into the same value of the dependent variable y for -1 < y < 1, and one value of x gives is mapped into one value of y for y < -1 and y > 1. For the inverse of this function each value of  $\gamma$  corresponds to either one or three values of x. The original cubic function, now viewed from the side, gives the appearance of being folded over twice on itself. In like manner, one lets T be the identity mapping of the extended object plane onto an image plane that is folded over on itself twice, with the two folds joined together in a pleat (see, for example, Fig. 4 of [18], Fig. 4 of [19], and Fig. 5 of [16]). The evolution of the image of an extended object traversing a path in the  $(x_e, y_e)$  plane across the two fold-lines of the distorted image plane is analyzed in the same way as for the 0-to-2 image transition, and reproduces the results given earlier in this section.

### 6. SUMMARY

The image of small bubbles on the back surface of a water-filled cylinder, or an extended object placed a small distance behind it, can both be easily viewed by an observer and exhibit much interesting structure. The real and virtual portions of the transmission rainbow caustic of a near-zone source and the behavior of scattering glare points are both necessary for understanding the image of a small bubble on the rear inside surface of a waterfilled cylinder. The bubble may be considered as an effective point source, whose transmitted light forms an exterior caustic. When an observer focuses his or her eyes in the vicinity of the cylinder, the rays triangulated back to their effective crossing location lie on the caustic and appear as glare points. As the observer's head is moved past the deflection angle of the transmission rainbow of the near-zone source, the two glare point images on the observer's retina of the same bubble take on color, merge together, and then vanish.

The image of an extended object a small distance behind the cylinder may be understood using the caustic touching theorem, which describes the topological method of fragmentation of an object's image into multiple images. By considering light traveling backwards from the observer's retina to the extended object plane, the imaginary cylindrical aberration caustic of the water-filled cylinder decomposes the extended object plane into a three-ray region sandwiched between two one-ray regions. As the first point of an extended object moves across the imaginary caustic from one of the one-ray regions into the three-ray region, an image-pair creation event occurs, producing two new partial images joined together back-to-back. When the last point of the extended object crosses the imaginary caustic, an image-pair disconnection event occurs, separating the now complete two conjoined images and producing three complete images. Similarly, when the first point on the extended object moves across the imaginary caustic from the three-ray region into the other one-ray region, an image-pair merging event occurs, where two of the images become joined together backto-back. When the last point on the extended object crosses the boundary, an image-pair annihilation event occurs, causing the final point on the conjoined images to vanish and producing one remaining complete image. It is a sign of the richness of these easily observed phenomena that the interplay of a large number of different optical structures is required for their understanding.

**Disclosures.** The author declares no conflict of interest.

#### REFERENCES

- 1. R. A. R. Tricker, *Introduction to Meteorological Optics* (American Elsevier, 1970).
- J. Walker, "How to create and observe a dozen rainbows in a single drop of water," Sci. Am. 237, 138–144 (1977).
- 3. J. D. Walker, "Multiple rainbows from single drops of water and other liquids," Am. J. Phys. **44**, 421–433 (1976).
- 4. J. A. Lock, "Theory of the observations made of high-order rainbows from a single water droplet," Appl. Opt. 26, 5291–5298 (1987).
- H. C. van de Hulst and R. T. Wang, "Glare points," Appl. Opt. 30, 4755–4763 (1991).
- 6. W. J. Humphreys, Physics of the Air (Dover, 1964).

- C. B. Boyer, The Rainbow: from Myth to Mathematics (Princeton University, 1987).
- H. M. Nussenzveig, "The theory of the rainbow," Sci. Am. 236, 116–127 (1977).
- J. A. Lock and T. A. McCollum, "Further thoughts on Newton's zeroorder rainbow," Am. J. Phys. 62, 1082–1089 (1994).
- J. E. McDonald, "Caustic of the primary rainbow," Am. J. Phys. 31, 282–284 (1963).
- P.-E. Ouellette, "Supernumerary bows: caustics of a refractive sphere and analysis of the relative overall Gouy phase shift of supernumerary rays," Appl. Opt. 58, 712–722 (2019).
- 12. P.-E. Ouelette, "Geometric optics of a refringent sphere illuminated by a point source: caustics, wavefronts, and zero phase-fronts for every rainbow 'k' order," J. Opt. Soc. Am. **35**, 1–11 (2018).
- M. V. Berry, "Disruption of images: the caustic-touching theorem," J. Opt. Soc. Am. A4, 561–569 (1987).
- J. F. Nye, Natural Focusing and Fine Structure of Light (Institute of Physics, 1999).
- 15. J. W. Goodman, Introduction to Fourier Optics (McGraw-Hill, 1968).
- J. Walker, "Caustics: mathematical curves generated by light shined through rippled plastic," Sci. Am. 249, 190–201 (1983).
- 17. A. B. Fraser and W. H. Mach, "Mirages," Sci. Am. **234**, 102–111 (1976)
- 18. W. Tape, "The topology of mirages," Sci. Am. 252, 120-129 (1985).
- W. Tape, "Folds, pleats, and halos," Am. Sci. 70, 467–474 (1982), and reprinted in Geometrical Aspects of Scattering, SPIE Milestone Series, Marston, P. L., ed., Vol. MS89 (SPIE, 1994), pp. 705–712.
- J. A. Lock and E. A. Hovenac, "Internal caustic structure of illuminated liquid drops," J. Opt. Soc. Am. A8, 1541–1552 (1991).
- 21. D. Halliday, R. Resnick, and J. Walker, *Fundamentals of Physics*, 7th ed. (Wiley, 2005).
- M. V. Berry, "Singularities in waves and rays," in *Physics of Defects*,
   R. Balian, M. Kléman, and J.-P. Poirier, eds. (North-Holland, 1981),
   pp. 453–543.
- H. M. Nussenzveig, "High-frequency scattering by a transparent sphere. I. Direct reflection and transmission," J. Math. Phys. 10, 82–124 (1969).
- J. A. Lock, "Semiclassical scattering of an electric dipole source inside a spherical particle," J. Opt. Soc. Am. 18, 3085–3097 (2001).
- C. L. Adler, J. A. Lock, J. Mulholland, B. Keating, and D. Ekelman, "Experimental observation of total-internal-reflection rainbows," Appl. Opt. 42, 406–411 (2003).
- M. V. Berry, "Reflections on a Christmas-tree bauble," Phys. Ed. 7, 1–6 (1972).
- J. A. Lock, "Role of the tunneling ray in near-critical-angle scattering by a dielectric sphere," J. Opt. Soc. Am. A20, 499–507 (2003).
- 28. J. A. Lock and P. Laven, "The Debye series and its use in time-domain scattering," in *Light Scattering Reviews*, A. Kokhanovsky, ed. (Springer-Praxis, 2016), Vol. **11**, pp. 219–297.
- R. Greenler, Rainbows, Halos, and Glories (Cambridge University, 1980).
- M. S. Longuet-Higgins, "Reflection and refraction at a random moving surface. I. Pattern and paths of specular points," J. Opt. Soc. Am. 50, 838–844 (1960).
- D. K. Lynch, D. S. P. Dearborn, and J. A. Lock, "Glitter and glints on water," Appl. Opt. **50**, F39–F49 (2011).
- D. Falk, D. Brill, and D. Stork, Seeing the Light, Optics in Nature, Photography, Color, Vision, and Holography (Harper & Row, 1986).
- P. Schneider and A. Weiss, "The two-point-mass lens: detailed investigation of a special asymmetric gravitational lens," Astron. Astrophys. 164, 237–259 (1986).
- K. Daněk and D. Heyrvoský, "Critical curves and caustics of triple-lens models," Astrophys. J. 806, 99 (2015).